An ab Initio and Density Functional Study of Al_3As, Al_3As^-, $AlAs_3$, and $AlAs_3^-$

Edet F. Archibong and Alain St-Amant*

Department of Chemistry, University of Ottawa, P.O. Box 450, Stn. A, 10 Marie Curie, Ottawa, Ontario, Canada K1N 6N5

Received: March 21, 2002; In Final Form: May 30, 2002

The low-lying electronic states of Al_3As, $AlAs_3$, and the corresponding anions have been studied at the B3LYP and CCSD(T) levels using the 6-311+G(*2df*) one-particle basis set. The ground electronic states of Al_3As^- and Al_3As have a cyclic planar C_{2v} geometry. A $^1A_1$-(C_{3v}) state is located 0.2 eV above the $^1A_1$-(C_{2v}) ground state of Al_3As. For $AlAs_3$, a near degeneracy is found between the $^1A_1$ (C_{2v}) and the $^1A'$ (C_s) lowest states while the anion, $AlAs^-$, has a $^2A'$ (C_s) ground state. The adiabatic electron affinities of Al_3As and $AlAs_3$ are calculated to be 1.8 and 1.9 eV, respectively. Electron detachment energies computed for the anions and the harmonic vibrational frequencies of both the anions and the neutral molecules are presented and discussed. It is anticipated that the computed data will aid future analysis and the interpretation of experimental photoelectron photodetachment spectra of these systems.

1. Introduction

A systematic and detailed study of the electronic structure of small clusters of AlP, GaP, and InP were recently reported by Neumark and co-workers,[1−5] following the pioneering work on the electronic structure of small GaAs clusters by Smalley and co-workers[6−9] and the matrix infrared experiments on diatomic and triatomic phosphides and arsenides of gallium by Weltner and his associates.[10] Advancing the efforts to understand the evolution of geometric and electronic properties as a function of size in binary group 13−15 clusters, Neumark's group has employed the anion photodetachment photoelectron technique to measure the vertical electron detachment energies (VEDE) and the electron affinities (EA) of several group 13−15 binary clusters, some of them having up to 27 atoms. From the differences in the VEDE of the anions, the authors have obtained estimates of the energy separation for several low-lying electronic states of the neutral clusters. In some cases, in addition to term values, they have also been able to extract frequencies from spectra that exhibit vibrational resolution.[1−3] According to the literature, their work on the electronic structure of AlP and GaP clusters represents the first experimental spectroscopic studies reported for the size of molecules they have studied.[1−5]

Complementing the photoelectron experiments are several computational studies that have broadened our understanding of the geometric and electronic properties of the group 13−15 clusters. In fact, quite a few of the computational studies predate some of the reported anion photodetachment photoelectron experiments. For example, Bruna and Grein, in a detailed and meticulous MRD-CI study,[11] predicted the electron photodetachment transitions of AlP^- well in advance of the recent work in Neumark's group. In the same vein, theoretical work by Peyerimhoff, Grein, and their collaborators on gallium arsenides containing up to four atoms,[12,13] those by Raghavachari and co-workers on $(AlP)_n$ clusters and Ga_4As_4,[14,15] and the work by Balasubramanian's group on small clusters of AlP and GaP,[16] have all been very useful in the analysis and interpretation of the observed spectra of these systems.

* Corresponding author. Fax: +1-613-5625170. E-mail: st-amant@theory.chem.uottawa.ca.

Despite the numerous experimental and theoretical investigations on the GaAs, InAs, InP, and more recently, the AlP and GaP clusters, the literature contains very little on the AlAs clusters. Recently, Feng et al. reported MRSDCI study of the ground and several low-lying excited states of Al_2As_3, Al_3As_2, and their ions,[17] thereby extending ab initio electronic structure calculations of the group 13−15 clusters to include the arsenides of aluminum. We note that prior to the computational study of the five-atom AlAs clusters reported in ref 17, Quek et. al. had reported[18] tight binding molecular dynamics studies of the structures of Al_mAs_n ($m + n \leq 13$) and Andreoni had studied AlAs clusters within the ab initio Car-Parrinelo molecular dynamics framework.[19] The purpose of this study is to extend computational studies of the binary group 13−15 clusters to the four-atom complexes, Al_3As and $AlAs_3$.

Therefore, continuing our work on oxides, phosphides, and arsenides of Al and Ga,[20−23] this article reports the B3LYP and CCSD(T) studies of the ground and low-lying excited states of Al_3As and $AlAs_3$ and their negative ions. The central objective is to predict the gas-phase equilibrium geometry of the anions and the neutral molecules, and then compute the VEDE and the adiabatic electron detachment energies (AEDE) for transitions originating from the lowest-lying states of the anions to some of the neutral states that can be accessed in a photodetachment experiment. In addition to calculating the energy separation for the low-lying electronic states, harmonic vibrational frequencies are reported to guide the interpretation of vibrationally resolved spectra.

2. Computational Methods

The 6-311+G(*2df*) basis set[24] is used for all the calculations. For Al, the basis consists of McLean and Chandler (*12s9p*)/[*6s5p*] contracted Gaussian-type functions (CGTF), augmented with two sets of five-membered *d*-type functions [ζ(Al) = 0.65, 0.1625], a set of diffuse *sp* functions [ζ(Al) = 0.0318;] and a seven-membered set of *f* functions [ζ(Al) = 0.25]. The As basis set was developed by Curtiss et. al.[25] It consists of an [8*s*7*p*2*d*] contracted set augmented with two sets of five-membered *d*-type functions [ζ(As) = 0.528, 0.132], a set of diffuse *sp* functions

10.1021/jp020779u CCC: $22.00
Published on Web 07/19/2002

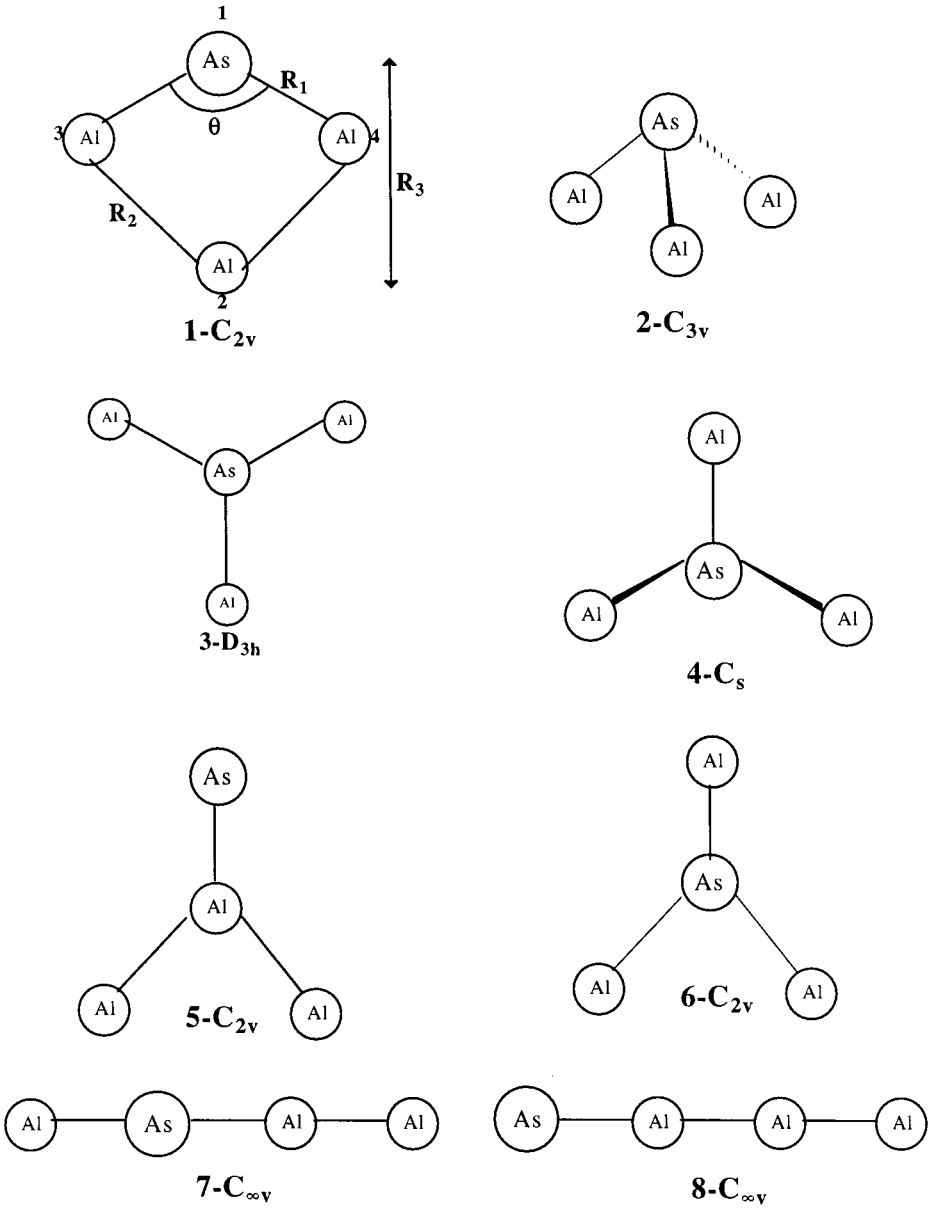

Figure 1. Structures of Al_3As and Al_3As^- reported in Tables 1 and 2.

[ζ(As) = 0.026], and a single set of seven-membered *f*-type functions [ζ(As) = 0.42]. Therefore, a [7*s*6*p*2*d*1*f*] and a [9*s*8*p*4*d*1*f*] set is placed on each Al and As center, respectively, to give a total of 186 and 222 CGTFs on Al_3As/Al_3As^- and $AlAs_3/AlAs_3^-$, respectively. The approach followed in this study involves using the hybrid B3LYP density functional and the MP2 method for full geometry optimizations. In addition, the geometries of the lowest-lying states of Al_3As are optimized at the CCSD(T) level. For all stationary points located on the B3LYP and MP2 potential surfaces, single-point energy calculations are carried out at the CCSD(T) level using the DFT and MP2 geometries. Frequency calculations at the B3LYP level, and in some cases at the MP2 level, are used to characterize the stationary points as minima, first- or higher-order saddle points. For the MP2 and CCSD(T) calculations, the 29 and 47 lowest molecular orbitals (MO) are frozen for Al_3As/Al_3As^- and $AlAs_3/AlAs_3^-$, respectively. No virtual orbitals are deleted in any of the calculations. All the computations are performed with the GAUSSIAN 98 suite of programs.[26]

3. Results and Discussion

The structures initially considered for geometry optimization are obtained from several sources. For example, the XAl_3^- (X = Si, Ge, Sn, and Pb) aromatic species[27,28] of Boldyrev and Wang (BW) and XAl_3 (X = P, As, Sb, Bi) are valence isoelectronic. BW have established that the most stable isomer of XAl_3^- (X = Si, Ge, Sn, and Pb) is the planar C_{2v} structure labeled as **1**-C_{2v} in Figure 1, followed by the pyrimidal C_{3v} isomer labeled in the figure as **2**-C_{3v}. Consequently, potential candidates for the gas-phase equilibrium geometry of Al_3As are **1**-C_{2v} and **2**-C_{3v}. Support for **1**-C_{2v} as the most likely ground-state structure for Al_3As comes from the DFT-LDA calculations of Lou et al.[29] in which **1** has been found to be the gas-phase structure of isovalent Ga_3As, and the tight binding molecular dynamics study of Al_3As that places **1** lowest in energy among several structures considered in that study.[18] In addition to **1** and **2**, we also consider other structures for geometry optimization and some of them are labeled 3−**8** in Figure 1. For $AlAs_3$, the guess structures are the most stable isomers reported in the tight binding molecular dynamics study of Quek et al.[18] Unless

TABLE 1: Total Energies, Adiabatic Energy Separations (ΔE, eV), Adiabatic Electron Detachment Energies (AEDE, eV), and Vertical Electron Detachment Energies (VEDE, eV) for Al_3As/Al_3As^-

cluster	method	structure	state	total energy	ΔE	AEDE	VEDE
Al_3As							
	CCSD(T)[b]	**8**-$C_{\infty v}$	$^1\Sigma^+$	−2960.197 528	2.73		
	CCSD(T)[b]	**5**-C_{2v}	$^1A_1$	−2960.212 502	2.32		
	CCSD(T)[a]	**1**-C_{2v}	$^3A_2$	−2960.239 658	1.60	3.38	3.59
	CCSD(T)[b]			−2960.239 616	1.59	3.39	3.59
	CCSD(T)[b]	**7**-$C_{\infty v}$	$^1\Sigma^+$	−2960.248 407	1.35		
	CCSD(T)[a]	**1**-C_{2v}	$^3A_1$	−2960.258 522	1.09		2.90
	CCSD(T)[b]			−2960.257 887	1.09		2.90
	CCSD(T)[a]	**1**-C_{2v}	$^3B_2$	−2960.262 995	0.96	2.74	2.96
	CCSD(T)[b]			−2960.262 848	0.95	2.75	2.95
	B3LYP	**3**-D_{3h}	$^1A_1'$	−2963.252 786	-0.05		
	MP2			−2960.230 918	0.49		
	CCSD(T)[a]			−2960.291 314	0.19		
	CCSD(T)[b]			−2960.291 314	0.18		
	MP2	**2**-C_{3v}	$^1A_1$	−2960.231 536	0.48		
	CCSD(T)[b]			−2960.291 784	0.17		
	CCSD(T)			−2960.291 796	0.18		
	B3LYP	**1**-C_{2v}	$^1A_1$	−2963.250 905	0.00	1.80	
	MP2			−2960.248 999	0.00	1.46	
	CCSD(T)[a]			−2960.298 446	0.00	1.78	2.02
	CCSD(T)[b]			−2960.297 898	0.00	1.80	2.02
	CCSD(T)			−2960.298 556	0.00		
Al_3As^-							
	CCSD(T)[b]	**1**-C_{2v}	$^2A_2$	−2960.323 653	1.10		
	CCSD(T)[b]	**1**-C_{2v}	$^2B_1$	−2960.339 770	0.66		
	CCSD(T)[b]	**6**-C_{2v}	$^2A_1$	−2960.340 598	0.64		
	CCSD(T)[b]	**4**-C_s	$^2A'$	−2960.342 295	0.59		
	CCSD(T)[b]	**1**-C_{2v}	$^2A_1$	−2960.349 109	0.41		
	B3LYP	**1**-C_{2v}	$^2B_2$	−2963.317 206	0.00		
	MP2			−2960.302 481	0.00		
	CCSD(T)[a]			−2960.364 030	0.00		
	CCSD(T)[b]			−2960.364 042	0.00		

[a] Computed with B3LYP geometry. [b] Computed with MP2 geometry.

indicated otherwise, the calculations reported in the sections below employ the 6-311+G(*2df*) basis set and the relative energies (ΔE) listed in the tables do not include corrections for zero-point energies.

3.1. Al_3As and Al_3As^-. Figure 1 is a sketch of the structures considered for Al_3As in this study. The adiabatic energy separation, (ΔE), between the electronic states of Al_3As are presented in Table 1. The table also includes VEDE and AEDE for Al_3As^-. Selected geometric parameters and harmonic vibrational frequencies for the lowest-lying states of Al_3As and Al_3As^- are listed in Table 2.

Inspection of Table 1 shows that three states, the $^1A_1$ (**1**-C_{2v}), $^1A_1$ (**2**-C_{3v}), and $^1A_1'$ (**3**-D_{3h}) states are potential candidates for the ground electronic state of Al_3As. At the MP2 level, a $^1A_1$ (**1**-C_{2v}) ground state is predicted for Al_3As with $^1A_1$ (**2**-C_{3v}) and the $^1A_1'$ (**3**-D_{3h}) states higher in energy by roughly 0.5 eV. Vibrational frequency analysis at this level, however, indicates that $^1A_1'$ (**3**-D_{3h}) is a transition state connecting two equivalent forms of **2**-C_{3v} with a low inversion barrier less than 0.02 eV. On the other hand, both $^1A_1$ (**1**-C_{2v}) and $^1A_1'$ (**3**-D_{3h}) are true minima on the B3LYP potential surface with **3** slightly more stable by 0.05 eV. The $^1A_1$ (**2**-C_{3v}) state could not be found with B3LYP, the optimization procedure always converged to **3**-D_{3h}. Energies of the three lowest-lying states of Al_3As are subsequently refined at the CCSD(T) level. First, CCSD(T) single-point energy calculations using the MP2 and B3LYP geometries, that is, CCSD(T)//MP2 and CCSD(T)//B3LYP, respectively, place the $^1A_1$ (**2**-C_{3v}) and $^1A_1'$ (**3**-D_{3h}) states within 0.17−0.19 eV above the $^1A_1$ (**1**-C_{2v}) state. With full geometry optimization of **1** and **2** at the CCSD(T) level, the $^1A_1$ (**1**-C_{2v}) state is established as the ground electronic state of Al_3As with the $^1A_1$ (**2**-C_{3v}) state higher in energy by 0.18 eV. Note that in a recent study by us, **1** is slightly above **2** by 0.07 and 0.13 eV for Al_3P and Ga_3P, respectively, at the CCSD(T)/6-311+G(*2df*) level.[30,31] In this study, **1** is found to be the most stable isomer of Al_3As just as it is for Ga_3As.[31] The relative stability of **1** and **2** for the M_3X (M = Al, Ga; X = P, As) system, appears to mirror the trend established for the valence isoelectronic XAl_3^- (X = Si, Ge, Sn, and Pb).[27,28] That is, **1** becomes more stable as X becomes heavier. Results of our study on the relative stability of **1** and **2** in M_3X (M = Al, Ga, In; X = P, As, Sb, Bi) will be communicated soon.

In addition to the lowest-lying singlet states discussed in the preceding paragraph, the $^1\Sigma^+$ (**7**-$C_{\infty v}$), $^1A_1$ (**5**-C_{2v}), $^1\Sigma^+$ (**8**-$C_{\infty v}$) are found at 1.35, 2.32, and 2.73 eV above the $^1A_1$ (**1**-C_{2v}) ground state at the CCSD(T)//MP2 level. Excited triplet states with the **1**-C_{2v} geometry are $^3B_2$ (0.95 eV), $^3A_1$ (1.09 eV) and $^3A_2$ (1.59 eV). Note the small separation (∼0.15 eV) between the $^3B_2$ and the $^3A_1$ states. The energy separation between these triplets and corresponding singlets, having the same electronic configuration, will be discussed in section 3.1.1. Selected geometric parameters for the triplet states and the harmonic vibrational frequencies are included in Table 2. The source of the anomalous frequencies (see Table 2) obtained for the ω_5 (b_2) and ω_6 (b_2) modes of the $^3A_1$ (**1**-C_{2v}) exited state has not been thoroughly investigated. Nonetheless, from our experience these are indications of problems in employing single reference correlated methods for the description of this particular state. A T_1 diagnostic of 0.037 at the CCSD level (using MP2 geometry) indicates a significant multiconfiguration character for the $^3A_1$ state.

The ground-state geometry of Al_3As^- is sought starting from the geometries optimized at the MP2 level for the neutral Al_3As isomers, that is, structures **1** through **8**. Because they are the lowest energy structure for the neutral, **1**-C_{2v} and **2**−C_{3v} are viable contenders for the gas-phase equilibrium structure of the anion. Accommodation of an extra electron by the b_2 lowest unoccupied MO (LUMO) of the $^1A_1$ (**1**-C_{2v}) state yields the $^2B_2$ (**1**-C_{2v}) [...$(6b_1)^2$ $(10b_2)^2$ $(18a_1)^2$ $(11b_2)^1$] state of Al_3As^-. A positive vertical electron affinity (VEA) of 1.44 eV is calculated for the $^1A_1$ (**1**-C_{2v}) → $^2B_2$ (**1**-C_{2v}) process. Note that the VEA of isovalent Al_3P at the same level of theory is 1.47 eV.[30] For **2**-C_{3v}, a ^2E state of the anion is expected to be formed if the neutral gains an electron. Jahn Teller distortion of the ^2E state will result in $^2A'$ (C_s) and $^2A''$ (C_s) states. Only the former is located at the MP2 level and the CCSD(T)//MP2 calculation places it 0.59 eV above the $^2B_2$ (**1**-C_{2v}) state. None of the doublet and quartet states of structures **6**−**8** are lower in energy than $^2B_2$ (**1**-C_{2v}). Three excited states with the **1**-C_{2v} geometry are found to be stable with respect to electron detachment. They are located 0.41 eV ($^2A_1$), 0.66 eV ($^2B_1$), and 1.10 eV ($^2A_2$) above the $^2B_2$ state. In short, our study of the Al_3As^- potential energy surface finds a $^2B_2$ (**1**-C_{2v}) ground state for the anion. The fragmentation energies are 5.31 eV for Al_3As^- [$^2B_2$ (C_{2v})] → Al_3 ($^2A_1'$) + As^- (^3P) and 8.93 eV for Al_3As^- [$^2B_2$ (C_{2v})] → 3Al (^2P) + As^- (^3P). In the case of Al_3As, they are 4.09 eV for Al_3As [$^1A_1$ (C_{2v})] → Al_3 ($^2A_1'$) + As (^4S) and 7.71 eV for Al_3As [$^1A_1$ (C_{2v})] → 3Al (^2P) + As (^4S).

3.1.1. Electron Detachment Transitions: Al_3As^-. One-electron detachment from the $11b_2$ highest occupied MO (HOMO) of

TABLE 2: Geometries (Å, degrees), Vibrational Frequencies (cm^{-1}), and Zero-Point Energies (ZPE, kcal/mol) for the Low-Lying States of Al_3As^- and Al_3As

	Al_3As^- $^2B_2$ (**1**-C_{2v})	Al_3As $^1A_1$ (**1**-C_{2v})	Al_3As $^3B_2$ (**1**-C_{2v})	Al_3As $^3A_1$ (**1**-C_{2v})	Al_3As $^3A_2$ (**1**-C_{2v})	Al_3As $^1A_1$ (**2**-C_{3v})	Al_3As $^1A_1'$ (**3**-D_{3h})
MP2							
R_1	2.450	2.396	2.536	2.398	2.585	2.454	2.445
R_2	2.690	2.553	2.792	2.821	2.760		
R_3	2.644	3.063	2.373	2.601	2.801		
θ_1	127.2	108.2	138.4	137.1	123.0	111.1	
θ_2	109.4	98.9	116.3	104.7	110.8		
ω_1	327 (a_1)	358 (a_1)	393 (a_1)	339 (a_1)	280 (a_1)	299 (a_1)	290 (a_1')
ω_2	224 (a_1)	277 (a_1)	219 (a_1)	251 (a_1)	188 (a_1)	40 (a_1)	334 (e′)
ω_3	132 (a_1)	157 (a_1)	107 (a_1)	126 (a_1)	136 (a_1)	323 (e)	43 (e′)
ω_4	95 (b_1)	120 (b_1)	58 (b_1)	85 (b_1)	311 (b_1)	53 (e)	29*i*
ω_5	325 (b_2)	362 (b_2)	295 (b_2)	1458[a]	268 (b_2)		
ω_6	262 (b_2)	347 (b_2)	128 (b_2)	239*i*	223 (b_2)		
ZPE	1.95	2.32	1.72	3.20	2.0	1.56	1.49
B3LYP							
R_1	2.447	2.371	2.529	2.443	2.598		2.448
R_2	2.695	2.630	2.796	2.785	2.776		
R_3	2.647	3.057	2.401	2.612	2.839		
θ_1	127.5	112.5	138.1	133.5	122.4		
θ_2	109.0	97.2	115.2	107.4	110.2		
ω_1	316 (a_1)	344 (a_1)					279 (a_1')
ω_2	204 (a_1)	234 (a_1)					322 (e′)
ω_3	142 (a_1)	130 (a_1)					58 (e′)
ω_4	69 (b_1)	99 (b_1)					9 (a_2'')
ω_5	315 (b_2)	337 (b_2)					
ω_6	248 (b_2)	280 (b_2)					
ZPE	1.85	2.04					1.50
CCSD(T)							
R_1		2.389			2.455		
R_2		2.616					
R_3		3.065					
θ_1		111.4			112		
θ_2		97.9					

[a] Large unphysical intensites obtained for this mode.

the $^2B_2$ (**1**-C_{2v}) [...$(6b_1)^2$ $(10b_2)^2$ $(18a_1)^2$ $(11b_2)^1$] ground electronic state of Al_3As^- is expected to yield a $^1A_1$ (C_{2v}) state of Al_3As. Detaching an electron from HOMO-1, HOMO-2, and HOMO-3 will result in the formation of the ($^3B_2$, $^1B_2$), ($^3A_1$, $^1A_1$), and ($^3A_2$, $^1A_2$) states. VEDE and AEDE for transitions to the triplet states of the neutral are easily calculated using the single-reference based theoretical methods employed in this work, but the corresponding open-shell singlet states cannot be described adequately by these methods. Estimates of the VEDE for transitions to the singlet states are obtained as follows. A time-dependent DFT (TDDFT) calculation employing the B3LYP functional is carried out for each singlet−triplet pair (for example $^1B_2$ and $^3B_2$) at the optimized ground-state geometry of Al_3As^-. The singlet−triplet splitting from the TDDFT calculation is then added to the VEDE computed for the triplet at the CCSD(T) level.

In a recorded electron photodetachment photoelectron spectrum of Al_3As^-, the following one-electron detachment processes from the $^2B_2$ (**1**-C_{2v}) [...$(6b_1)^2$ $(10b_2)^2$ $(18a_1)^2(11b_2)^1$] ground electronic state of Al_3As^- to neutral Al_3As may be observed. In this discussion, the molecule is placed on the Y−Z plane with the *Z*-axis passing through As−Al2.

(A) $^1A_1$ *(*C_{2v}*)* $+ e^- \leftarrow$ $^2B_2$ *(*C_{2v}*).* Removal of an electron from the $11b_2$ HOMO of Al_3As^- yields the $^1A_1$ (C_{2v}) [...$(6b_1)^2$ $(10b_2)^2$ $(18a_1)^2$] ground state of Al_3As. At the CCSD(T)//B3LYP and CCSD(T)//MP2 level, the VEDE for this transition is 2.02 eV. Because the $^1A_1$ (C_{2v}) ← $^2B_2$ (C_{2v}) process involves the ground states of the anion and the neutral, the AEDE for this transition is equivalent to the adiabatic electron affinity (AEA) of Al_3As. Its value is calculated to be 1.78 eV at the CCSD(T)//B3LYP level and 1.80 eV at the CCSD(T)//MP2 level. Although both the anion and the neutral have the **1**-C_{2v} equilibrium geometry, their respective geometric parameters are quite different as manifested clearly in the ∼0.23 eV difference between the VEDE and the AEDE. Also, the harmonic vibrational frequencies computed for the anion show significant differences with respect to their neutral counterparts. The vacated $11b_2$ MO consists essentially of As (p_y), Al2(p_y), Al3(s,p_y), and Al4(s,p_y). Using the B3LYP results, electron detachment to the $^1A_1$ state of the neutral results in a pronounced 0.41 Å elongation of the As−Al2 distance with a shortening of the equivalent As−Al bond lengths by 0.08 Å and the Al−Al distance by 0.07 Å. In addition, the AlAsAl and the AlAlAl angles are substantially compressed by 15° and 12°, respectively. Because of the large geometry change involving these angles when going from the anion to the neutral, in a recorded spectrum, ω_2 (a_1) and ω_3 (a_1) involving the AlAsAl and AlAlAl bending modes (with some contributions from Al−Al stretching) are expected to be dominant for the $^1A_1$ band. The frequencies of these totally symmetric modes are included in Table 2.

(B) $^3B_2$ *(*C_{2v}*)* $+ e^- \leftarrow$ $^2B_2$ *(*C_{2v}*).* Electron detachment from the $18a_1$ MO of the anion yields the $^3B_2$ state and the $^1B_2$ state. For the $^3B_2$ state, the VEDE and the AEDE are 2.95 and 2.75 eV, respectively, at the CCSD(T)//MP2 level. The CCSD(T) calculation places this triplet state 0.95 eV above the $^1A_1$ ground state. A singlet−triplet (S-T) splitting of 0.35 eV is obtained from the TDDFT calculation and from this value, the VEDE for the $^1B_2$ (C_{2v}) $+ e^-$ ← $^2B_2$ (C_{2v}) process is approximated to be 3.30 eV. The equivalent As−Al3/As−Al4 bonds and the Al−Al bond are 0.08 and 0.10 Å, respectively, longer for the

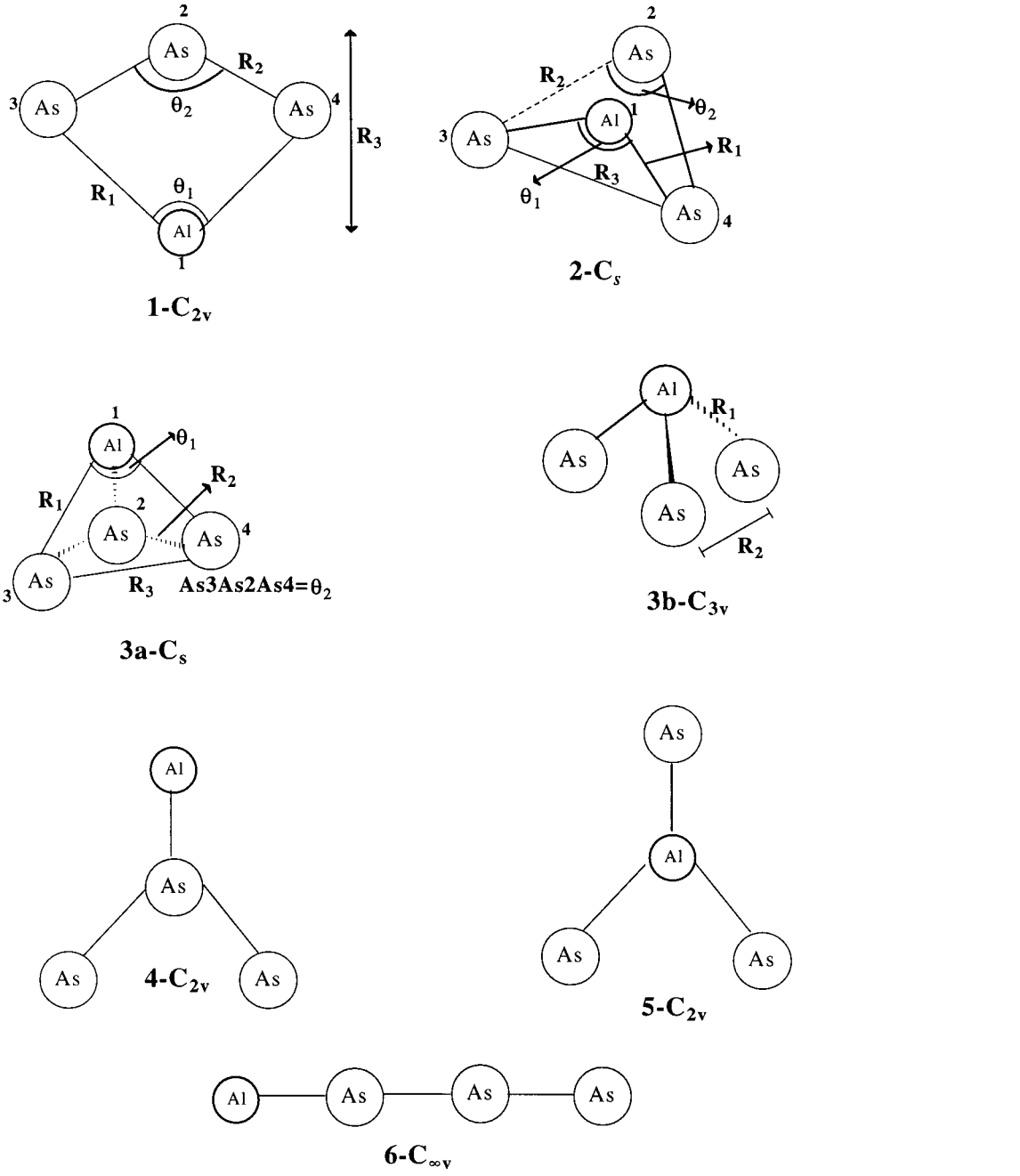

Figure 2. Structures of $AlAs_3$ and $AlAs_3^-$ reported in Tables 3 and 4.

$^3B_2$ state than in the anion, indicating the bonding character of the $18a_1$ MO which essentially consists of As (s,p_z), Al2 (s), Al3 (s,p_y), and Al4(s,p_y). Apparently, the largest geometry change between the anion ground state and the $^3B_2$ state involves shortening of the diagonal As−Al2 distance by 0.27 Å and an increase of 11° in the AlAsAl angle. Consequently, the $^3B_2$ band is expected to be dominated by a progression with a frequency of ca. 393 cm^{-1} corresponding to the ω_1 AlAsAl bending mode of the $^3B_2$ state.

(C) $^3A_1$ *(*C_{2v}*)* + e^- ← $^2B_2$ *(*C_{2v}*).* The $10b_2$ MO is a four-center orbital with relatively strong Al−Al bonding character. It consists mainly of As (p_y), Al2 (p_y), Al3 (s,p_y), and Al4 (s,p_y). Removal of an electron from the $10b_2$ MO of the anion is expected to yield the $^3A_1$ (C_{2v}) and $^1A_1$ (C_{2v}) states. At the CCSD(T) level, the VEDE for the $^3A_1$ ← $^2B_2$ transition is 2.90 eV. Note that the latter is lower than 2.95 eV obtained for the $^3B_2$ ← $^2B_2$ transition. However, after geometry optimization, the $^3B_2$ state is 0.14 eV lower than the $^3A_1$ state. From the TDDFT calculation, 0.70 eV is obtained for the $^1A_1$−$^3A_1$ splitting, and from this, the VEDE for the $^1A_1$ + e^- ← $^2B_2$ transition is approximated to be 3.60 eV. As noted in section 3.1, anomalous frequencies and intensities are obtained for the ω_5 (b_2) and ω_6 (b_2) modes of the $^3A_1$ exited state. This could be due to interaction with close-lying electronic states and the inability of the single-reference MP2 method to describe this triplet state appropriately. Consequently, the VEDE computed for the $^3A_1$ + e^- ← $^2B_2$ and the $^1A_1$ + e^- ← $^2B_2$ processes can only be regarded as estimates at best.

(D) $^3A_2$ *(*C_{2v}*)* + e^- ← $^2B_2$ *(*C_{2v}*).* The $6b_1$ MO of Al_3As^- ($^2B_2$ state) is a delocalized out-of-plane π bonding orbital consisting largely of As (p_x) and contributions from p_x orbitals of the three Al atoms in the ring. We note that this MO closely resembles the $1b_1$ MO which is responsible for the stability and the proposed π-aromatic character of **1**-C_{2v} in XAl_3^- (X = Si, Ge, Sn, and Pb).[27,28] This π-MO is also found in **1**-C_{2v} of Al_3P and Ga_3P but is less delocalized than observed here for Al_3As and

TABLE 3: Total Energies (a.u) and the Energy Separations (ΔE, eV) for $AlAs_3/AlAs_3^-$

			CCSD(T)[a]		CCSD(T)[b]	
cluster	structure	state	total energy	ΔE	total energy	ΔE
$AlAs_3$						
	6-$C_{\infty v}$	$^1\Sigma^+$			−6944.857 223	2.22
	5-C_{2v}	$^1A_1$			−6944.886 112	1.43
	4-C_{2v}	$^1A_1$	−6944.892 636	1.25	−6944.892 816	1.25
	3b-C_{3v}	$^1A_1$	−6944.896 775	1.14	−6944.896 960	1.14
	1-C_{2v}	$^3A_2$	−6944.904 478	0.93	−6944.903 889	0.95
	1-C_{2v}	$^3B_2$	−6944.905 600	0.90	−6944.905 280	0.91
	2-C_s	$^3A'$	−6944.916 595	0.60	−6944.916 422	0.61
	3b-C_{3v}	$^3A_2$	−6944.917 558	0.58	−6944.917 579	0.57
	3a-C_s	$^1A'$	−6944.920 886	0.49	−6944.921 082	0.48
	1-C_{2v}	$^1A_1$	−6944.938 075	0.02	−6944.937 845	0.02
	2-C_s	$^1A'$	−6944.938 744	0.00	−6944.938 675	0.00
$AlAs_3^-$						
	1-C_{2v}	$^2B_1$	−6944.997 021	0.35	−6944.996 741	0.33
	1-C_{2v}	$^2A_1$	−6944.996 981	0.35	−6944.996 800	0.33
	3b-C_{3v}	$^2A_1$	−6945.005 042	0.13	−6945.004 969	0.11
	3a-C_s	$^2A''$	−6945.007 324	0.07	−6945.007 234	0.05
	2-C_s	$^2A'$	−6945.009 979	0.00	−6945.009 038	0.00

[a] CCSD(T)//B3LYP. [b] CCSD(T)//MP2.

in Ga_3As.[31] Electron detachment from the $6b_1$ MO is expected to yield the $^3A_2$ and the $^1A_2$ states. The VEDE for the $^3A_2$ (C_{2v}) + $e^- \leftarrow {}^2B_2$ transition is 3.59 eV and the AEDE is 3.39 eV at the CCSD(T)//MP2 level. The triplet state is found 1.59 eV above the $^1A_1$ ground state. A $^1A_2-{}^3A_2$ splitting of 0.20 eV from TDDFT allows us to approximate the VEDE for the $^1A_2$ + $e^- \leftarrow {}^2B_2$ transition to be 3.79 eV. The $^3A_2$ band in the photodetachment spectrum of Al_3As^- is expected to exhibit progressions involving the ω_1 (a_1) Al−As stretching (frequency 280 cm^{-1}, MP2) and the ω_2 (a_1) Al−Al stretching (frequency 188 cm^{-1}, MP2) modes. This is consistent with the bonding character of the π-MO which on ionization results in Al−As and Al−Al bond lengthening of 0.14 and 0.07 Å, respectively.

3.2. $AlAs_3$ and $AlAs_3^-$. From the tight binding molecular dynamics study of AlAs clusters by Quek et al., **1**-C_{2v} (see Figure 2) appears to emerge as the most stable isomer of $AlAs_3$.[18] The current study investigates the singlet and the triplet potential energy surfaces of $AlAs_3$ and the results are listed in Tables 3 and 4. Based on the relative energies in Table 3, **1**-C_{2v} and **2**-C_s are the most stable isomers of $AlAs_3$. The **2**-C_s ($^1A'$) form can be described as a distorted tetrahedron in which the As3AlAs4 plane makes a 109° (B3LYP) [107° (MP2)] angle to the As3As2As4 plane. At the B3LYP and MP2 levels, both **1**-C_{2v} ($^1A_1$) and **2**-C_s ($^1A'$) are true minima having only real harmonic vibrational frequencies. However, the energies of these lowest-lying isomers of $AlAs_3$ are too close to allow unequivocal establishment of their relative order. Within the CCSD(T)// B3LYP and CCSD(T)//MP2 approximations, **2**-C_s ($^1A'$) is found 0.02 eV (∼0.5 kcal/mol) below **1**-C_{2v} ($^1A_1$). Allowing for intrinsic errors of about 2 kcal/mol in these calculations, the inference that can be drawn is that the $^1A'$ (**2**-C_s) and $^1A_1$ (**1**-C_{2v}) states of $AlAs_3$ are nearly degenerate. Using the CCSD-(T)//MP2 results, the following states are found above the $^1A'$ (**2**-C_s) state: $^1A_1$ (**1**-C_{2v}, 0.02 eV), $^1A'$ (**3a**-C_s, 0.48 eV), $^3A_2$ (**3b**-C_{3v}, 0.57 eV), $^3A'$ (**2**-C_s, 0.61 eV), $^3B_2$ (**1**-C_{2v}, 0.91 eV), $^3A_2$ (**1**-C_{2v}, 0.95 eV), $^1A_1$ (**3b**-C_{3v}, 1.14 eV), $^1A_1$ (**4**-C_{2v}, 1.25 eV), and $^1\Sigma^+$ (**6**-$C_{\infty v}$, 2.22 eV). The geometric parameters and the harmonic vibrational frequencies for the lowest-lying states are included in Table 4. At the CCSD(T)//B3LYP level, the fragmentation energies are 2.82 eV for $AlAs_3$ ($^1A'$) → Al (^2P) + As_3 ($^2A_2$), 2.65 eV for $AlAs_3$ ($^1A'$) → AlAs ($^3\Sigma^-$) + As_2 ($^1\Sigma_g^+$), 2.94 eV for $AlAs_3$ ($^1A'$) → $AlAs_2$ ($^2B_2$) + As (^4S), and 8.12 eV for $AlAs_3$ ($^1A'$) → Al (^2P) + 3As (^4S).

The search for the gas-phase equilibrium geometry of $AlAs_3^-$ is conducted starting with the lowest energy structures located on the potential energy surface of $AlAs_3$. Several stationary points are located for the anion and Tables 3 and 4 include the energies, geometric parameters, and the harmonic vibrational frequencies of the lowest-lying states. Analogous to its neutral counterpart, the two lowest states of $AlAs_3^-$ are separated by less than 2 kcal/mol. At the CCSD(T)//MP2 level, the $^2A'$ (**2**-C_s) state is 0.05 eV lower than the $^2A''$ (**3a**-C_s) state. The geometry of the former resembles that of $^1A'$ (**2**-C_s) state of the neutral except that the As3AlAs4 plane is almost perpendicular (92° B3LYP, 84° MP2) to the As3As2As4 plane. For the $^2A''$ (**3a**-C_s) state, the angle between the As3AlAs4 plane and the As3As2As4 plane is narrower (63° B3LYP, 65° MP2), the Al−As2 distance shorter and its structure is best described as a distorted trigonal pyramid. At the B3LYP and MP2 levels, the Hessian index (HI) is zero for the optimized geometry of the $^2A'$ (**2**-C_s) state. On the other hand, as indicated in Table 4, the optimized geometry of $^2A''$ (**3a**-C_s) possesses an HI of one and zero at the B3LYP and MP2 levels, respectively.

In addition to the nearly degenerate $^2A'$ (**2**-C_s) and $^2A''$ (**3a**-C_s) states, a $^2A_1$ state with the pyramidal **3b**-C_{3v} geometry is computed for the anion. Frequency calculations indicate that **3b**-C_{3v} ($^2A_1$) is a local minimum on both the MP2 and B3LYP potential energy surfaces and lies 0.11 eV [CCSD(T)//MP2] above **2**-C_s ($^2A'$). Low-lying excited states of the anion having the **1**-C_{2v} structure are also studied. Both the $^2B_1$ (**1**-C_{2v}) and $^2A_1$ (**1**-C_{2v}) states have almost the same energy. They are 0.33 eV above the $^2A'$ (**2**-C_s) state at the CCSD(T)//MP2 level. At the MP2 level, **1**-C_{2v} ($^2A_1$) is a local minimum while **1**-C_{2v} ($^2B_1$) is a first-order saddle point. Distortion and subsequent geometry optimization of the latter results in **2**-C_s.

In summary, using the 6-311+G(*2df*) one-particle basis set, the $^1A'$ (**2**-C_s) and $^1A_1$ (**1**-C_{2v}) lowest-lying states of $AlAs_3$ are separated by roughly 0.02 eV (∼0.5 kcal/mol) at the CCSD-(T)//B3LYP and CCSD(T)//MP2 levels. However, all the theoretical models used in this study appear to favor, albeit slightly, a $^1A'$ (**2**-C_s) ground state for the neutral molecule. Similarly, the $^2A'$ (**2**-C_s) and $^2A''$ (**3a**-C_s) states of $AlAs_3^-$ are within 0.05 eV of each other and at least two excited states of the anion, $^2A_1$ (**3b**-C_{3v}, 0.11 eV) and $^2A_1$ (**1**-C_{2v}, 0.33 eV) are stable with respect to electron detachment.

3.2.1. Electron Detachment Transitions: $AlAs_3^-$. The photodetachment photoelectron spectrum of $AlAs_3^-$ is expected to be very rich and unfortunately congested, a consequence of the several low-lying states of the anion and the neutral molecule. Some of the features expected in the spectrum are easily predicted using the results listed in Tables 3−5. The frequencies listed in Table 4 for the low-lying states might facilitate the interpretation of a vibrationally resolved spectrum. Table 5 lists the calculated VEDE for several one-electron processes involving the low-lying states of the anion. In this section, we discuss electron detachment processes originating from the $^2A'$ (**2**-C_s) and $^2A''$ (**3a**-C_s) nearly degenerate states of $AlAs_3^-$ (A−C) and summarize transitions that may involve the low-lying excited states of the anion.

*(A) $^1A'$ (**2**-C_s) + $e^- \leftarrow {}^2A'$ (**2**-C_s).* The $^2A'$ (C_s) ground state of the anion has a $[...(34a')^2(22a'')^2(35a')^1]$ electronic configuration. Detachment of an electron from the 35 a' orbital yields the $^1A'$ (C_s) $[...(34a')^2(22a'')^2]$ state. At the CCSD(T)//MP2 level, the VEDE for this process is 2.43 eV while the CCSD(T)// B3LYP value is 2.20 eV. This transition involves ground states of the anion and the neutral and consequently, the AEDE is equivalent to the AEA of $AlAs_3$ $^1A'$ (C_s). A value of 1.91 eV

TABLE 4: Geometries (Å, degrees), Vibrational Frequencies (cm^{-1}), and Zero-Point Energies (ZPE, kcal/mol) for the Low-Lying States of $AlAs_3^-$ and $AlAs_3$

	$AlAs_3^-$ $^2A'$ (**2**-C_s)	$AlAs_3^-$ $^2A''$ (**3a**-C_s)	$AlAs_3^-$ $^2A_1$ (**3b**-C_{3v})	$AlAs_3^-$ $^2A_1$ (**1**-C_{2v})	$AlAs_3^-$ $^2B_1$ (**1**-C_{2v})	$AlAs_3$ $^1A'$ (**2**-C_s)	$AlAs_3$ $^3A'$ (**2**-C_s)	$AlAs_3$ $^3A_2$ (**3b**-C_{3v})	$AlAs_3$ $^1A_1$ (**3b**-C_{3v})	$AlAs_3$ $^1A_1$ (**1**-C_{2v})	$AlAs_3$ $^3B_2$ (**1**-C_{2v})	$AlAs_3$ $^3A_2$ (**1**-C_{2v})
MP2												
R_1	2.606	2.777	2.455	2.481	2.336	2.508	2.429	2.835	2.365	2.400	2.312	2.490
R_2	2.376	2.491	2.517	2.343	2.428	2.354	2.427	2.404	2.632	2.331	2.458	2.334
R_3	2.566	2.344		2.738	2.639	2.689	2.634			2.570	2.716	2.897
θ_1	59.0	49.9		106.1	116.0	64.9	65.7			111.6	115.7	101.3
θ_2	65.4	56.1		115.7	109.4	69.7	65.7			116.8	105.6	111.2
ω_1	341 (a')	349 (a')	424 (a_1)	327 (a_1)	363 (a_1)	347 (a')	419 (a')	341 (a_1)	450 (a_1)	362 (a_1)	383 (a_1)	311 (a_1)
ω_2	296 (a')	304 (a')	265 (a_1)	240 (a_1)	215 (a_1)	274 (a')	296 (a')	247 (a_1)	219 (a_1)	223 (a_1)	252 (a_1)	255 (a_1)
ω_3	196 (a')	248 (a')	272 (e)	151 (a_1)	185 (a_1)	197 (a')	212 (a')	272 (e)	338 (e)	202 (a_1)	176 (a_1)	138 (a_1)
ω_4	124 (a')	183 (a')	184 (e)	287 (b_1)	80*i* (b_1)	151 (a')	171 (a')	170 (e)	141 (e)	124 (b_1)	77*i*	130*i*
ω_5	256 (a'')	837 (a'')[a]		362 (b_2)	445 (b_2)	276 (a'')	311 (a'')			412 (b_2)	488 (b_2)	333 (b_2)
ω_6	71 (a'')	192 (a'')		231 (b_2)	222 (b_2)	247 (a'')	82 (a'')			269 (b_2)	251 (b_2)	233 (b_2)
ZPE	1.83	3.02	2.29	2.29	2.04	2.13	2.13	2.10	2.33	2.28	2.22	1.82
B3LYP												
R_1	2.578	2.845	2.453	2.495	2.321	2.549	2.438	2.896	2.350	2.372	2.324	2.523
R_2	2.404	2.505	2.536	2.352	2.478	2.338	2.450	2.410	2.644	2.357	2.490	2.361
R_3	2.565	2.350		2.804	2.561	2.689	2.652			2.591	2.727	2.965
θ_1	59.7	48.8		104.6	118.7	63.7	66.2			113.0	116.8	100.3
θ_2	64.5	56.0		114.1	107.4	70.2	65.5			114.1	105.3	110.3
ω_1	332 (a')	325 (a')	407 (a_1)	300 (a_1)	340 (a_1)	340 (a')	388 (a')	330 (a_1)	448 (a_1)	347 (a_1)	336 (a_1)	290 (a_1)
ω_2	279 (a')	293 (a')	255 (a_1)	231 (a_1)	209 (a_1)	275 (a')	280 (a')	222 (a_1)	217 (a_1)	217 (a_1)	208 (a_1)	238 (a_1)
ω_3	196 (a')	230 (a')	261 (e)	144 (a_1)	166 (a_1)	184 (a')	185 (a')	234 (e)	337 (e)	206 (a_1)	161 (a_1)	133 (a_1)
ω_4	107 (a')	160 (a')	165 (e)	183*i*	123*i*	142 (a')	152 (a')	49 (e)	139 (e)	126 (b_1)	109*i*	175*i*
ω_5	237 (a'')	138*i*		316 (b_2)	435 (b_2)	265 (a'')	287 (a'')			401 (b_2)	433 (b_2)	291 (b_2)
ω_6	156 (a'')	181 (a'')		208 (b_2)	187 (b_2)	197 (a'')	24 (a'')			229 (b_2)	221 (b_2)	212 (b_2)
ZPE	1.85	1.70	2.16	1.71	1.91	2.00	1.88	1.60	2.31	2.18	1.94	1.66

[a] Intensity of this mode is unphysical (3778 km/mol).

TABLE 5: Energies (a.u) of Neutral Species at Anion Geometry, Vertical Electron Detachment Energies (VEDE, eV) of $AlAs_3^-$, and the Adiabatic Electron Affinity (AEA, eV) $AlAs_3$

structure	initial state	final state	method	energy[a]	VEDE	AEA
2-C_s	$^2A'$	$^1A'$	CCSD(T)//B3LYP	-6944.929 025	2.20	1.94
			CCSD(T)//MP2	-6944.919 644	2.43	1.91
		$^3A''/^3A_2(C_{3v})$				
			CCSD(T)//B3LYP	-6944.907 688	2.78	
			CCSD(T)//MP2	-6944.907 959	2.75	
		$^3A'$				
			CCSD(T)//B3LYP	-6944.903 435	2.90	
			CCSD(T)//MP2	-6944.905 332	2.82	
3b-C_{3v}						
	$^2A_1$	^3E	CCSD(T)//B3LYP	-6944.906 673	2.68	
			CCSD(T)//MP2	-6944.907 181	2.66	
		$^1A_1$				
			CCSD(T)//B3LYP	-6944.890 497	3.12	
			CCSD(T)//MP2	-6944.888 937	3.16	
1-C_{2v}						
	$^2A_1$	$^1A_1$	CCSD(T)//B3LYP	-6944.932 494	1.75	
			CCSD(T)//MP2	-6944.934 826	1.69	
		$^3A_2$				
			CCSD(T)//B3LYP	-6944.903 423	2.55	
			CCSD(T)//MP2	-6944.901 935	2.58	

[a] Energy of neutral at the geometry of the anion; the total energies of the anions and the neutral molecules are listed in Table 3.

is calculated for the AEA at the CCSD(T)//MP2 level and 1.94 eV at the CCSD(T)//B3LYP level. Although the anion and the neutral have the same molecular symmetry, the substantial difference between the VEDE and the AEDE is a consequence of the significant change in geometry when the 35 a' orbital is vacated. The latter MO is As3−As4 bonding. Removal of an electron from the anion to produce the $^1A'$ (C_s) state lengthens the As3−As4 bond by 0.12 Å and the As3AlAs4 and As3As2As4 angles widen by roughly 4° and 6°, respectively. If the $^1A'$ band is vibrationally resolved, the ω_3 mode (As3−As4 stretching with some contributions from As3AlAs4 and As3As1As4 bending) is expected to be active. The ω_3 frequency is calculated to be 184 cm^{-1} using the B3LYP functional and 197 cm^{-1} at the MP2 level.

(B) $^3A''$ (**2**-C_s) + $e^- \leftarrow$ $^2A'$ (**2**-C_s). Electron detachment from the 22a'' HOMO-1 of $AlAs_3^-$ $^2A'$ (C_s) is expected to yield the $^3A''$ (C_s) [...(34a')^2(22a'')^1(35a')^1] state and the open-shell $^1A''$ (C_s) state of neutral $AlAs_3$. For the $^3A''$ (C_s) + $e^- \leftarrow$ $^2A'$ (C_s) process, the VEDE is 2.75 eV at the CCSD(T)//MP2 level and 2.78 eV at the CCSD(T)//B3LYP level. Subsequent geometry optimization at the MP2 level converged to the pyramidal **3b**-C_{3v} structure. The AEDE of 2.49 eV for the $^3A_2$ (**3b**-C_{3v}) $\leftarrow$ $^2A'$ (**2**-C_s) transition places $^3A_2$ (C_{3v}) 0.57 eV above the $^1A'$ (C_s) ground state of $AlAs_3$. A broad band is expected for this

transition because of the large geometry change between the anion (C_s) and the neutral (C_{3v}). Harmonic vibrational frequencies for the C_{3v} ($^3A_2$) isomer are included in Table 4.

(C) $^3A'$ (**2**-C_s) + e^- ← $^2A'$ (**2**-C_s). Removal of an electron from the 34*a*′ HOMO-2 of $AlAs_3^-$ $^2A'$ (C_s) yields the $^3A'$ (C_s) and $^1A'$ (C_s) excited states of $AlAs_3$. Both have the [...(34*a*′)^1-(22*a*″)^2(35*a*′)^1] electronic configuration. The process resulting in the $^3A'$ (C_s) state has a VEDE of 2.82 eV at the CCSD(T)//MP2 level and 2.90 eV at the CCSD(T)//B3LYP level. This transition is accompanied by As3−As4 bond lengthening (0.087 Å B3LYP, 0.068 Å MP2) in accordance with the bonding character of the 34*a*′ MO. At the CCSD(T)//MP2 level, the AEDE for the $^3A'$ (**2**-C_s) + e^- ← $^2A'$ (**2**-C_s) process is calculated to be 2.52 eV.

In addition to the detachment of electrons from the nearly degenerate $^2A'$ (**2**-C_s) and $^2A''$ (**3a**-C_s) states of $AlAs_3^-$, the following processes, involving the low-lying excited states, might also give rise to features in the observed spectrum. From the $^2A_1$ (**3b**-C_{3v}) [...(16*a*)^2(17*a*)^1(18*e*)^2] state, the ^3E (**3b**-C_{3v}) and the $^1A_1$ (**3b**-C_{3v}) states result via detachment from the 18*e* or 17*a* MO, respectively. Using the CCSD(T)//MP2 results, the VEDE for the ^3E (**3b**-C_{3v}) + e^- ← $^2A_1$ (**3b**-C_{3v}) process is 2.66 and 3.16 eV for $^1A_1$ (**3b**-C_{3v}) + e^- ← $^2A_1$ (**3b**-C_{3v}).

The photoelectron spectrum of $AlAs_3^-$ may also exhibit lower binding energy features due to the **1**-C_{2v} isomer. As mentioned in section 3.2, the most stable forms of $AlAs_3$, the **2**-C_s ($^1A'$) and **1**-C_{2v} ($^1A_1$) forms, are separated by roughly 0.02 eV (∼0.5 kcal/mol). The low-lying $^1A_1$ (**1**-C_{2v}) state of $AlAs_3$ is formed by removing the electron in the 25a_1 HOMO of $^2A_1$ (**1**-C_{2v})-[...(17b_2)^2(6a_2)^2(25a_1)^1]. Detaching an electron from the 6a_2 HOMO-1 yields the $^3A_2$ (**1**-C_{2v}) state. With the molecule on the Y−Z plane (*Z*-axis passing through Al−As2), the HOMO consists of Al (s,p_z), As2(s,p_z), As3(p_z), As4(p_z), and its antibonding character results in appreciable Al−As2 bond lengthening (0.17 Å MP2, 0.21 Å B3LYP) of the neutral. The principal components of HOMO-1 are the p_x orbitals of As3 and As4, and the orbital is nonbonding. For the $^1A_1$ (**1**-C_{2v}) + e^- ← $^2A_1$ (**1**-C_{2v}) process, the VEDE (1.75 eV CCSD(T)//B3LYP, 1.69 eV CCSD(T)//MP2) is well below (2.20 eV CCSD(T)//B3LYP, 2.43 eV CCSD(T)//MP2) that calculated for the $^1A'$ (**2**-C_s) + e^- ← $^2A'$ (**2**-C_s) transition involving ground states of the anion and the neutral. In the case of the $^3A_2$ (**1**-C_{2v}) + e^- ← $^2A_1$ (**1**-C_{2v}) transition, the VEDE is 2.58 eV at the CCSD(T)//MP2 level and 2.55 eV at the CCSD(T)//B3LYP level. Because the $^1A_1$ (**1**-C_{2v}) + e^- ← $^2A_1$ (**1**-C_{2v}) transition is accompanied by a significant change in the Al−As2 bond distance, if observed, the $^1A_1$ (**1**-C_{2v}) band might exhibit extended progressions in the ω_1 and ω_2 modes (symmetric ring stretchings). At the MP2 level, the frequencies for these modes are 362 and 223 cm^{-1}, respectively, and the corresponding B3LYP values are 347 and 217 cm^{-1}.

Finally, it is appropriate to compare a segment of our results for Al_3As and $AlAs_3$ with those obtained for their isovalent (Al_3P/Ga_3As and AlP_3/$GaAs_3$) counterparts in early studies.[30,32,33] Foremost, the most stable structure computed for Al_3As in this study is the planar **1**-C_{2v} ($^1A_1$) of Figure 1. On the other hand, Balasubramanian and co-workers found the pyramidal **2**-C_{3v} ($^1A_1$) to be the lowest energy structure for Al_3P and Ga_3As.[32,33] It is noteworthy that the relative stability of **1**-C_{2v} ($^1A_1$) and **2**-C_{3v} ($^1A_1$) is not reported in refs 32 and 33 for Al_3P and Ga_3As, respectively. However, a more recent study[30] has shown that while **1**-C_{2v} ($^1A_1$) and **2**-C_{3v} ($^1A_1$) of Al_3P have almost the same energy, it is the planar **1**-C_{2v} isomer that is responsible for Al_3P^- photodetachment spectrum.[1] It is surprising that for Ga_3As^-, only one state ($^2A_2$-C_{2v}) is reported to be stable with respect to electron loss and a comparatively low AEA of 1.077 eV (MRSDCI) has been calculated for the Ga_3As molecule. The AEA calculated for Ga_3As using DFT-LDA is 1.3 eV.[29] In contrast, for Al_3As^-, several states are found to be stable toward electron detachment (see Table 1) and the AEA of Al_3As is calculated to be 1.80 eV at the CCSD(T)//MP2 level. The latter AEA is close to a value of 1.78 eV calculated for Al_3P.[30] From our results, we predict that several features observed in the anion photodetachment spectrum of Al_3P^- will also be found in the spectra of Al_3As^- and Ga_3As^-.

In the case of $AlAs_3$ and $AlAs_3^-$, their equilibrium geometry (**2**-C_s in Figure 2) is similar to that found[33] for $GaAs_3$/$GaAs_3^-$ but differs from the pyramidal C_{3v} structure suggested for AlP_3.[32] For $GaAs_3$, the ground state is reported to be well separated from the $^3A_2$ (C_{3v}) lowest excited state by 0.5 eV.[33] However, the results listed in Table 3 shows that for $AlAs_3$, the lowest states are $^1A_1$ (C_{2v}) and $^1A'$ (C_s) and they are nearly degenerate. While the AEA computed for $GaAs_3$ is 1.48 eV at the MRSDCI level,[33] a value of 1.91 eV is computed for $AlAs_3$ at the CCSD-(T)//MP2 level. It is hoped that the results presented in this work and some of the similarities and differences listed above will help in future experiments on these group 13−15 semiconductor clusters.

4. Conclusions

In this paper, the equilibrium geometries, harmonic vibrational frequencies and the relative energies of the low-lying states of the neutral and anionic forms of Al_3As and $AlAs_3$ are presented and discussed for the first time. As a primary objective, we have also described electron detachment processes from the lowest-lying states of the anions to several states of the neutral, to guide future experimental anion photodetachment photoelectron studies.

Acknowledgment. We thank the Natural Sciences and Engineering Research Council of Canada and the University of Ottawa for financial support.

References and Notes

(1) Gómez, H.; Taylor, T. R.; Neumark, D. M. *J. Phys. Chem. A* **2001**, *105*, 6886.
(2) Taylor, T. R.; Gómez, H.; Asmis, K. R.; Neumark, D. M. *J. Chem. Phys.* **2001**, *115*, 4620.
(3) Taylor, T. R.; Asmis, K. R.; Gómez, H.; Neumark, D. M. *Eur. Phys. J. D* **1999**, *9*, 317.
(4) Asmis, K. R.; Taylor, T. R.; Neumark, D. M. *Chem. Phys. Lett.* **1999**, *308*, 347.
(5) Taylor, T. R.; Asmis, K. R.; Xu, C.; Neumark, D. M. *Chem. Phys. Lett.* **1998**, *297*, 133.
(6) O'Brien, C.; Liu, Y.; Zhang, Q. L.; Heath, J. R.; Tittel, F. K.; Curl, R. F.; Smalley, R. E. *J. Chem. Phys.* **1986**, *84*, 4074.
(7) Liu, Y.; Zhang, Q. L.; Tittel, F. K.; Curl, R. F.; Smalley, R. E. *J. Chem. Phys.* **1986**, *85*, 7434.
(8) Cheshnovsky, O.; Yang, S. H.; Pettiette, C. L.; Craycraft, M. J.; Liu, Y.; Smalley, R. E. *Chem. Phys. Lett.* **1987**, *138*, 119.
(9) Jin, C.; Taylor, K. J.; Conceicao, J.; Smalley, R. E. *Chem. Phys. Lett.* **1990**, *175*, 17.
(10) Li, S.; Van Zee, R. J.; Weltner, W., Jr. *J. Phys. Chem.* **1993**, *97*, 11393.
(11) Bruna, P. J.; Grein, F. *J. Phys. B: At. Mol. Opt. Phys.* **1989**, *22*, 1913.
(12) Meier, U.; Peyerimhoff, S. D.; Bruna, P. J.; Grein, F. *J. Mol. Spectrosc.* **1989**, *134*, 259.
(13) Meier, U.; Peyerimhoff, S. D.; Grein, F. *Chem. Phys.* **1991**, *150*, 331.
(14) Al-Laham, M. A.; Trucks, G. W.; Raghavachari, K. *J. Chem. Phys.* **1992**, *96*, 1137.
(15) Al-Laham, M. A.; Raghavachari, K. *J. Chem. Phys.* **1993**, *98*, 8770.
(16) Balasubramanian, K.; Feng, P. Y. *J. Phys. Chem. A* **2001**, *105*, 11295 and references therein.

(17) Feng, P. Y.; Dai, D.; Balasubramanian, K. *J. Phys. Chem. A* **2000**, *104*, 422.
(18) Quek, H. K.; Feng, Y. P.; Ong, C. K. *Z. Phys. D* **1997**, *42*, 309.
(19) Andreoni, W. *Phys. Rev. B* **1992**, *45*, 4203.
(20) Archibong, E. F.; St-Amant, A. *J. Phys. Chem. A* **1998**, *102*, 6877.
(21) Archibong, E. F.; St-Amant, A. *J. Phys. Chem. A* **1999**, *103*, 1109.
(22) Archibong, E. F.; St-Amant, *Chem. Phys. Lett.* **2000**, *330*, 199.
(23) Archibong, E. F.; St-Amant, A. *Chem. Phys. Lett.* **2002**, *355*, 249.
(24) (a) McLean, A. D.; Chandler, G. S. *J. Chem. Phys.* **1980**, *72*, 5639. (b) Krishnan, R.; Binkley, J. S.; Seeger, R.; Pople, J. A. *J. Chem. Phys.* **1980**, *72*, 650. (c) Clark, T.; Chandrasekhar, J.; Spitznagel, G. W.; Schleyer, P. v. R. *J. Comput. Chem.* **1983**, *4*, 294. (d) Frisch, M. J.; Pople, J. A.; Binkley, J. S. *J. Chem. Phys.* **1984**, *80*, 3265.
(25) Curtiss, L. A.; McGrath, M. P.; Blaudeau, J. P.; Davis, N. E.; Binning, R. C., Jr.; Radom, L. *J. Chem. Phys.* **1995**, *103*, 6104.
(26) Frisch, M. J.; Trucks, G. W.; Schlegel, H. B.; Scuseria, G. E.; Robb, M. A.; Cheeseman, J. R.; Zakrzewski, V. G.; Montgomery, J. A., Jr.; Stratmann, R. E.; Burant, J. C.; Dapprich, S.; Millam, J. M.; Daniels, A. D.; Kudin, K. N.; Strain, M. C.; Farkas, O.; Tomasi, J.; Barone, V.; Cossi, M.; Cammi, R.; Mennucci, B.; Pomelli, C.; Adamo, C.; Clifford, S.; Ochterski, J.; Petersson, G. A.; Ayala, P. Y.; Cui, Q.; Morokuma, K.; Malick, D. K.; Rabuck, A. D.; Raghavachari, K.; Foresman, J. B.; Cioslowski, J.; Ortiz, J. V.; Baboul, A. G.; Stefanov, B. B.; Liu, G.; Liashenko, A.; Piskorz, P.; Komaromi, I.; Gomperts, R.; Martin, R. L.; Fox, D. J.; Keith, T.; Al-Laham, M. A.; Peng, C. Y.; Nanayakkara, A.; Gonzalez, C.; Challacombe, M.; Gill, P. M. W.; Johnson, B. G.; Chen, W.; Wong, M. W.; Andres, J. L.; Head-Gordon, M.; E. S. Replogle, E. S.; Pople, J. A. *Gaussian 98*, revision A9; Gaussian, Inc.: Pittsburgh, PA, 1998.
(27) Li, Xi.; Zhang, H. F.; Wang, L. S.; Kuznetsov, A. E.; Cannon, N. A.; Boldyrev, A. I. *Angew. Chem., Int. Ed.* **2001**, *40*, 1867.
(28) Boldyrev, A. I.; Wang, L. S. *J. Phys. Chem. A* **2001**, *105*, 10759.
(29) Lou, L.; Nordlander, P.; Smalley, R. E. *J. Chem. Phys.* **1992**, *97*, 1858.
(30) Archibong, E. F.; St-Amant, A.; Goh, S. K.; Marynick, D. M., in press.
(31) Archibong, E. F.; St-Amant, A.; Goh, S. K.; Marynick, D. M. Submitted.
(32) Feng, P. Y.; Balasubramanian, K. *Chem. Phys. Lett.* **1999**, *301*, 458.
(33) Balasubramanian, K.; Zhu, X. *J. Chem. Phys.* **2001**, *115*, 8858.